TITAN MONTGOLFIERE BALLOON ANALYSIS AND DESIGN USING COMPUTATIONAL FLUID DYNAMICS SIMULATIONS

Jeffery L. Hall[(1)], Andre Vargas[(2)], Tim Colonius[(3)], Walter Dieudonné[(4)], Yuri Feldman[(5)], Jack A. Jones[(6)], Kim Reh[(7)] and Julian Nott[(8)]

[(1)]Jet Propulsion Laboratory, California Institute of Technology, 4800 Oak Grove Dr., Mail Stop 82-105, Pasadena, CA., USA, 91109. Email: jlhall@mail.jpl.nasa.gov
[(2)]CNES Centre National d'Etudes Spatiales, 18, Av. Edouard. belin, 31401 Toulouse cedex 9, France. Email: Andre.Vargas@cnes.fr
[(3)]California Institute of Technology, Mail Code 104-44, Pasadena, CA, USA, 91125 Email: colonius@caltech.edu
[(4)] Research in Technologies for Innovation in Modeling the Environment, 6 Résidence Chataigniers, 09000 Vernajoul, France. Email: walter.dieudonne@rtime.fr
[(5)]California Institute of Technology, Mail Code 104-44, Pasadena, CA, USA, 91125 Email: yurifeld@caltech.edu
[(6)]Jet Propulsion Laboratory, California Institute of Technology, 4800 Oak Grove Dr., Mail Stop 157-316, Pasadena, CA., USA, 91109. Email: jack.a.jones@jpl.nasa.gov
[(7)]Jet Propulsion Laboratory, California Institute of Technology, 4800 Oak Grove Dr., Mail Stop 321-625, Pasadena, CA., USA, 91109. Email: kreh@mail.jpl.nasa.gov
[(8)]Nott Technology LLC, 1482 East Valley Road, Santa Barbara, CA, USA 93108. Email: nott@nott.com

ABSTRACT

A Montgolfiere, or hot air balloon, is an attractive mobile platform for carrying scientific instruments on a wide-ranging exploration of Titan's lower atmosphere and surface regions. The key to successful implementation of the concept is an accurate prediction of buoyancy across the wide range of flight conditions expected on a long duration mission in the Titan environment. This paper reports on recent results from modeling thermo-fluid behavior of a Titan Montgolfiere using computational fluid dynamics (CFD) simulations. Many CFD simulations were performed, grouped into four categories that explored different aspects of the overall problem. First, Reynolds-averaged Navier-Stokes (RANS) techniques were used to model 1 meter diameter single and double wall balloons that were tested at cryogenic temperatures (90K) on Earth. Good agreement was obtained between the measured and simulated buoyancy for both balloons. Second, RANS models were used to simulate full scale (10 meter) double-wall balloon designs either as closed spheres or with realistic geometrical features such as a teardrop shape and an inlet hole at the bottom of the balloon. Although there were small differences between the closed sphere and realistic geometry computations, both sets of results showed that the double-wall design was less effective at increasing buoyancy than estimates based on engineering heat transfer correlations for concentric heated spheres held at uniform temperatures. This discrepancy led to the third group of simulations that focused on the thermo-fluid behavior of an idealized gap using direct and large-eddy simulation techniques that directly resolve the unsteady, turbulent convective flows for a Rayleigh (Ra) number range of $10^4 < Ra < 10^9$. Comparing these results to RANS simulations and correlations suggests that the engineering correlations do not provide accurate heat transfer estimates for the turbulent flow in thinner gaps under turbulent flow conditions. The fourth set of CFD simulations quantified the change in buoyancy performance due to forced external convection, modeling those flight conditions for a balloon with changing altitude. The paper concludes with a short parametric assessment that maps out the payload mass versus float altitude versus balloon size design space for full scale Titan Montgolfiere double-walled balloons using the heat transfer performance quantified by the recent CFD results. The basic conclusion is that the balloon diameter must grow by 10% to 20% to compensate for the poorer buoyancy performance indicated by the recent CFD simulations as compared to previous estimates based on correlations.

1. INTRODUCTION

There has been a tremendous amount of work done in recent years on the mission design and technology development aspects of a future balloon mission at Titan. Recent review articles by Lorenz [1], Dorrington [2] and Hall [3] summarize the balloon technology development activities and discuss the many different kinds of balloons and missions that are possible. The importance of continued Titan balloon technology development for a future mission was endorsed recently in the 2013-2023 Decadal Survey for Planetary Science. [4]

A Montgolfiere, or hot air, balloon is a leading concept for Titan. Figure 1 shows an artist's concept of such a balloon proposed for the Titan Saturn Systems Mission (TSSM) in 2008. [5] This Montgolfiere balloon would create buoyancy by heating up the

ambient atmosphere inside the balloon with waste heat from a radioisotope power source (RPS). The RPS would be located inside the balloon with ambient atmosphere entering through an opening in the bottom of the balloon. The buoyancy, and hence altitude, of the balloon would be controlled by a valve located on top of the balloon: when opened, that valve allows warm air to escape, decreasing buoyancy and causing the balloon to descend. When the valve is closed, the internal gas temperature and buoyancy increase, causing the balloon to ascend. A great advantage of such an RPS-powered Montgolfiere balloon is that it can potentially can fly for very long times, on the order of years, due to the long-lived RPS heat source and the insensitivity to small pinhole defects in the balloon envelope given that the balloon is already open to the atmosphere.

A key technical challenge of Titan Montgolfiere balloons is ensuring sufficient buoyancy generation under all flight conditions despite relatively small amounts of available thermal power. Terrestrial hot air balloons typically use propane burners to generate up to 100 kW of heat. Conversely, a Titan Montgolfiere balloon would have at most approximately 2 kW of heat by using a single multi-mission radioisotope thermal generator (MMRTG). Less heat than that would be available if the Advanced Stirling Radioisotope Generator (ASRG) were used instead of the MMRTG. It is plausible that 2 kW or less of thermal power will suffice at Titan because the 85-90 K cryogenic environmental temperature will almost completely suppress the heat loss due to thermal radiation, which is the primary loss mechanism on Earth. Heat losses can be further reduced by implementing a double-wall balloon design in which the air-filled gap between the walls serves as an insulating layer. The TSSM mission was based on this design [5].

Prior Titan Montgolfiere thermal designs, including TSSM, utilized engineering correlation equations based on laboratory experiments of small scale spheres (e.g. Scanlan, [6]). The performance estimates for such a design were necessarily approximate and with unknown errors given the lack of experimental data or more sophisticated models with which to compare. Full scale cryogenic testing is not expected to be possible given the lack of test facilities anywhere in the world that can accommodate a 10+ meter diameter balloon. Therefore, an alternative strategy was adopted by the authors to obtain improved performance estimates through use of computational fluid dynamics (CFD) simulations validated with small scale (1 meter diameter) cryogenic test data.

The results presented here build upon preliminary work published by some of the authors in the past two years. [7,8] The current work consists of four main areas of new research:

Fig. 1: Artist's concept of a double-wall Titan Montgolfiere balloon for the TSSM mission. [5]

1. Reynolds-averaged Navier-Stokes (RANS) techniques were used to model 1 meter diameter single and double wall balloons that were tested at cryogenic temperatures (90 K) on Earth.
2. RANS models were used to simulate full scale (10 meter) double-wall balloon designs either as closed spheres or with realistic geometrical features such as a teardrop shape and an inlet hole at the bottom of the balloon.
3. An idealized gap was simulated using direct and large-eddy simulation (LES) techniques to address discrepancies in the performance estimate between RANS and engineering correlations for gap heat transfer.
4. The effect of external forced convection was simulated to mimic balloon vertical motions.

The final section of the paper applies the CFD results to the problem of full scale Titan Montgolfiere balloon design and generates design curves of payload versus balloon size for different heating levels.

2. COMPUTATIONAL FLUID DYNAMICS RESULTS

2.1. Scaled Experimental and CFD analysis

In order to validate CFD models for the Titan Montgolfiere, experiments were performed on a scaled 1 m balloon in the Wyle Labs cryogenic facility, covering a range of ambient temperatures from 90-180 K. Both single- and double-walled balloons were tested. The double-walled balloon had a 5 cm gap between the inner and outer walls, which gives a ratio of inner to outer diameter of $D_i/D_o = 0.9$. The balloons were made buoyant by heating the gas with an electrical resistance heater, for which voltage and current to the heater were measured to determine the power input to the balloon. Thermocouples were embedded in the walls to measure skin temperature at several locations from crown to base and a load cell measured the lift of the balloon. A steel cylindrical shell was placed around the balloon within the cryogenic chamber to provide a quiescent atmosphere around the balloon during testing. A more detailed description of the experimental setup is provided in Feldman *et al*, [8]. Numerical simulations were performed at scale using commercial software Ansys12. [9] Turbulence was modeled via the Reynolds Averaged Navier Stokes (RANS) approach with a standard k−ε turbulence model and wall functions. The radiation modeling was switched off since, at this range of cryogenic temperatures, radiation effects are negligibly small. [8]

A comparison between experimental and numerical net buoyancy values for both single- and double-walled balloons is shown in Fig 2. There is consistently good agreement between simulation and experiment for both single- and double-walled configurations. The CFD generally predicts more buoyancy, and the differences increase as the ambient temperature is reduced (and the heat transfer rate increases), reaching a maximum of about 10% for single- and 15% for double-walled balloon at the external far field temperature T_∞ = 90 K. The overpredictions may be related to an imprecise modeling of the balloon's shape: the experimental balloons have a sphere-on-cone geometry while in the numerical simulations the balloons were idealized as a perfect sphere. Moreover, slight side-to-side movement of the balloons was observed during the experiment, indicative of small atmosphere currents not completely eliminated by the experimental setup.

The experimental and CFD results revealed an interesting effect of the small-scale geometry, namely a strong dependence of buoyancy on the temperature-dependent properties of the gas. Temperatures inside the small balloon can be as much as 200 K higher than ambient due to the high heat input values necessary to a achieve a substantial buoyancy force at small scale.

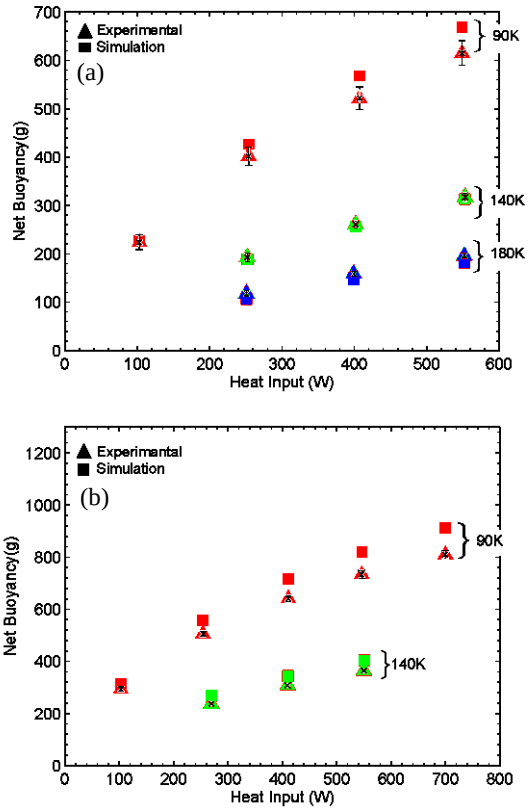

Fig. 2: Experimental and numerical buoyancy values: a) double-walled balloon; b) single- walled balloon.

The increasing viscosity and conductivity of the gas with temperature causes a significant increase in the heat transfer coefficient. Moreover, the temperature distribution varies strongly along the balloon surface (cold bottom/hot top). At large scale, the temperature differences are much smaller and the resulting temperature distribution is relatively more uniform. Thus there is a danger in extrapolating the experimental results to full scale. [8]

As discussed previously, the strong insulating effect of the gap in the double-walled design is critical to reduce the required heat input for a full-scale Montgolfiere at a given payload mass. In system-level models of the balloon heat transfer, the engineering correlation of Scanlan [6] is typically used to estimate the effective conductivity of the gap. This correlation is for concentric spheres with a uniform temperature difference. It is therefore of interest to compare the inferred effective conductivity of the gap from the CFD calculations to the value predicted by the correlation. Such a comparison is provided in Fig. 3, where the effective conductivity ratio, k_{eff}/k, is

plotted versus a modified Rayleigh number $Ra^* = RaL/R_i$, where Ra is the Rayleigh number based on the gap width L and gap temperature difference, $T_o - T_i$, i.e. $Ra = \frac{\beta g(T_o - T_i)L^3}{\upsilon\alpha}$. In processing the simulation data for the plot, average surface temperature were used. Values of k_{eff}/k obtained from simulations with different heat inputs, different ambient temperatures, and different gap widths collapse reasonably well on a power-law dependence in Ra^*, but the slope and interception differ significantly from the Scanlan correlation. The larger value of effective conductivity in the CFD results suggests that estimates of the insulating effect of the gap based on Scanlan will be overly optimistic.

One of the possible reasons for the discrepancy is the violation of basic assumptions inherent in the correlation, namely the constant temperature of the spherical shell boundaries. However, preliminary numerical simulations of the full-scale balloon on Titan, where the temperature differences from ambient are much smaller and more evenly distributed, show that a considerable discrepancy persists when comparing the effective conductivity measured in the simulations to the correlation. In order to resolve the discrepancy, we performed simulations of idealized gaps between concentric constant-temperature spheres across a wide range of conditions and with different modeling techniques. These results are presented in Section 2.3.

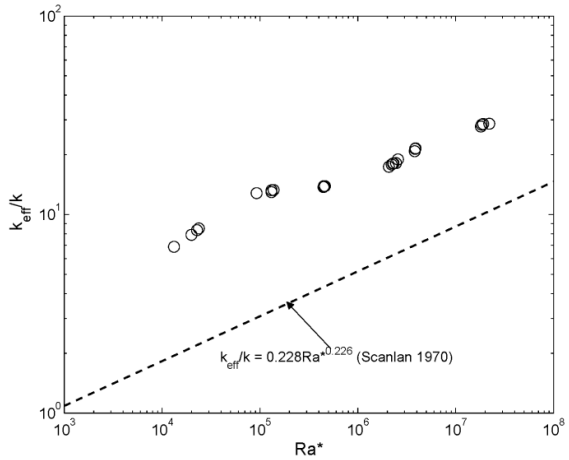

Fig. 3: Gap effective conductivity versus modified Ra* number. The symbols represent values inferred from the simulations of 1 m scaled balloons with a variety of heat inputs, ambient temperatures, and gap thicknesses.

2.2. Realistic balloon shapes, experimental rebuilding

So far, it was assumed that the 1 m diameter double wall balloon from the cryogenic experiment can be modeled as two concentric spheres. This is consistent with the geometry of the heat transfer correlations used in the 1D engineering models. The effect of modeling a real balloon shape is now considered for the CFD rebuilding and results will be compared to CFD rebuilding on equivalent spheres. The gap width between the inner and outer wall is kept at 0.05 m. In an additional study, the heat source location is varied within the balloon along the symmetry axis to check for the buoyancy sensitivity.

The flow conditions selected for this study correspond to the double wall, high heating case: P_a = 101200 Pa, T_a = 90 K, Q_{heater} = 550 W and U_∞ = 0 m/s. For the geometry, the spherical balloon has a 1 m diameter, an opening of 0.1 m and a gap width of 5 cm.

The real shape is obtained by digitizing a photograph taken during the experiment from which a few geometrical points have been reconstructed. From these points, a B-spline is constructed to ensure first and second order continuity; this defines the outer skin. The inner wall shape is obtained through a homothetic scaling using the area centroid as the origin. A view presenting the real balloon shape compared to the idealized spherical shape is showed in Fig. 4. The numerically constructed real balloon shape is compared to a photograph of the actual balloon taken during the Earth cryogenic experiment in Fig. 5.

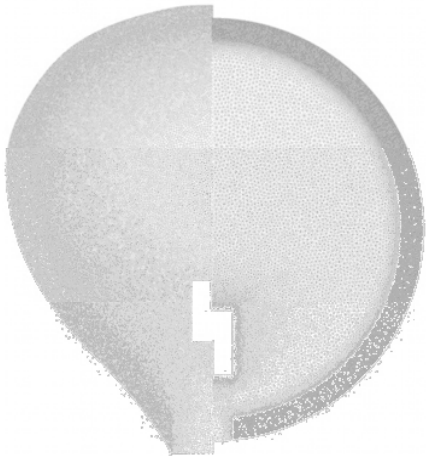

Fig. 4: comparison of real (left) and spherical balloon shapes (right), CFD grids.

Fig. 5: Comparison of numerically rebuilt (left) and cryogenic tests real balloon.

For the heater, a set of 3 locations is selected: from a very low location (baseline results), to a central location, to a high location (near the top). It is expected to get the highest buoyancy for the heater located the lowest as more inner volume is heated. The heater locations are shown in Fig. 66. The flow topology from a dynamic view point is unchanged when comparing the real shape to the spherical shape. However, the thermal plume length does necessarily shorten as the heater location is moved upwards towards the top of the balloon.

From the thermal field results (Fig. 7), lowering the heater location shows a more homogeneous flow (less stratified) and higher overall average temperature (more buoyancy). With the lowest heat location, one gets close to a 1D thermal flow within the balloon enclosure; the engineering convection correlations are based on that assumption. For the highest located heater, the vertical thermal gradient is the highest and the gap shows a thermal plume near the centerline leading to more heat loss (less buoyancy). As the heater is placed higher in the balloon, the thermal flow has two vertical nodes that are separated by the heater. The thermal field is presented in Fig. 7 for the three different heater locations.

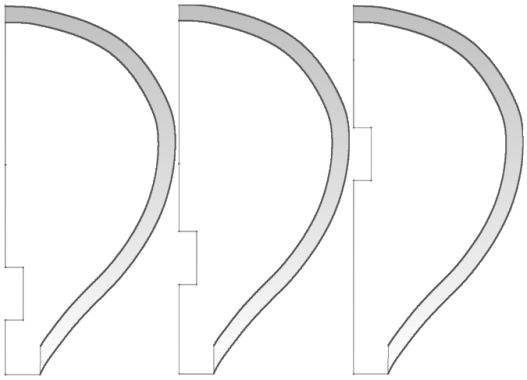

Fig. 6: heater location, from left to right: lowest (baseline), central, highest.

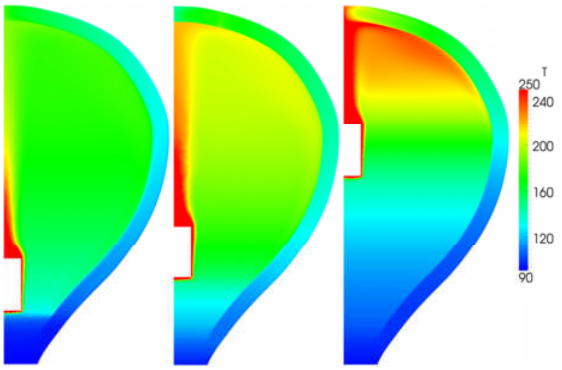

Fig. 7: thermal field on a shaped balloon with different heat source locations.

The buoyancy values for the real shape as a function of heater location for 550 W heat input are presented in Table 1. It is interesting to note that the volume to gap ratio does not change much. The inner volume is 0.342 m^3, the gap volume is 0.125 m^3 and the total volume is 0.467 m^3. The inner volume represents 73% of the total volume and the gap to total volume ratio is 27%. From the highest to the lowest heater location, the buoyancy varies by 15%.

Table 1 : Buoyancy values for the real shape double wall with the different contributions as a function of heater location. The spherical buoyancy reference value is 761 [g].

Heater location	Buoyant mass in grams [g]				
	Overall	Inner volume		Gap volume	
	m_{buoy}	m_{buoy}	%	m_{buoy}	%
Lowest	739	577.8	78.19%	161.2	21.81%
Central	717	561.0	78.24%	156.0	21.76%
Highest	628	500.9	79.76%	127.1	20.24%

Comparing the spherical shape buoyancy (m_{buoy}=761 g) with the baseline real shape buoyancy (m_{buoy}=739 g), one may note that the real shape produces slightly less buoyancy (~3%). Nevertheless, the values are close one another demonstrating that the spherical assumption used for the engineering correlations is valid.

2.3. Idealized gap heat transfer analysis

As discussed in the Section 2.1, CFD simulations of the scaled double-walled balloons showed significantly larger values of the gap effective conductivity than would be predicted based on the Scanlan correlation. [6] In order to investigate the discrepancy further, we now simulate the isolated, ideal gap between concentric spheres with an imposed

uniform temperature on each surface and a relatively small temperature differences between surfaces. This eliminates any uncertainty as to the effect of non-uniform wall temperatures and temperature-dependent property variations. Assuming constant gas properties the heat transfer, and specifically the effective gap conductivity, k_{eff}/k , is solely determined by the Ra and Pr numbers, and the ratio of inner-to-outer sphere diameter $\varphi = D_i/D_o$. According to Scanlan, the effective conductivity collapses to a universal curve when the diameter ratio and Ra are combined into $Ra^* = RaL/R_i$. In what follows, we hold $Pr = 0.71$ constant. We consider a range of values of Ra and φ that span the expected values of Ra^* for a full-scale Titan balloon design.

Moreover, to reduce uncertainties associated with turbulence modeling, we performed direct numerical simulation (DNS) and large-eddy simulation (LES) of the turbulent convective flow in the gap. DNS refers to a fully three-dimensional simulation where all the relevant (unsteady) scales of motion are directly resolved on the grid, and solved in parallel on a large computer cluster. The required grid size for DNS increases dramatically with Ra, and it is only feasible to use DNS for relatively small-scale gaps. To reach higher Ra, we turn to LES, which is a technique that resolves directly only the largest scales of turbulent motion and supplies a model to capture the dissipation associated with unresolved, small scales. We implemented both DNS and LES in OpenFoam. [10] For LES, we used a one-equation eddy viscosity model (a variation of the approach developed by Germano et al., [11]); further details will be given in forthcoming publications.

Figure 8 compares data for k_{eff}/k we obtained with DNS and LES to those obtained with the k − ε RANS model discussed in the Section 2.1, and to the Scanlan correlation. To provide further check of the

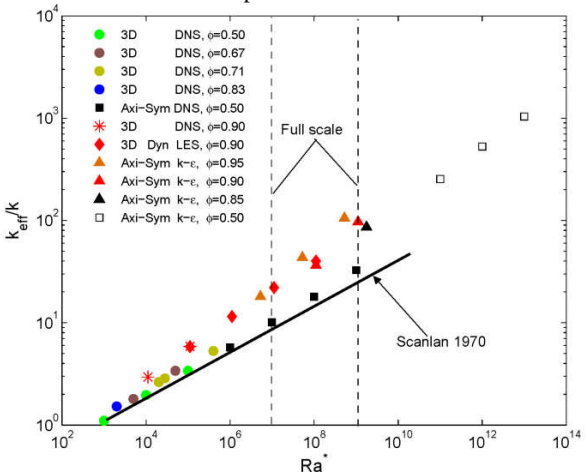

Fig. 8: Effective conductivity of the ideal gap versus modified Ra^*number.

the RANS results, we used both Ansys12 [9] and OpenFoam for the RANS simulations for several of the operating points, and obtained similar results. Figure 8, together with analysis of the resulting flow fields, reveals several interesting features of the gap convection. The first observation is that the values of Ra^* at which instability and transition to turbulence occur vary dramatically with gap ratio φ. For relatively low φ, the DNS simulations at low to moderate Ra^* resulted in laminar or quasi-laminar, unsteady flow, and relatively close agreement with the Scanlan correlation. The unsteady quasi-laminar flows consist of convection cells in the form of travelling waves and falling vortices. Turbulent flows were obtained for the thickest gap (φ = 0.5) only when $Ra^* > 10^9$. The thin gaps, on the other hand, transitioned at progressively smaller values of Ra^*. The hot gas rising on the inner sphere and the cold gas falling on the outer sphere form a strong shear layer instability in the middle of the gap.

The plot shows a clear departure from Scanlan once the gaps are turbulent. Looking at the thin gaps, and particularly the series of DNS and LES calculations for $\varphi = 0.9$, we see a similar intercept but higher slope than Scanlan. We found that at $Ra^* = 10^4$, the $\varphi = 0.9$ gap is only marginally turbulent, whereas it appears that transition is essentially complete by $Ra^* = 10^5$. The DNS and LES simulations at $Ra^* = 10^5$ are in very close agreement, which serves as a validation of the LES methodology.

We now turn to the RANS results. RANS modeling of the fully turbulent flow is challenging because the very thin boundary layers cannot be resolved on the coarse grid, and so-called wall functions must be used. However, such wall functions are only appropriate in the higher Ra number regime; when RANS is used at lower values of Ra^*, the wall model must be modified or switched off entirely. We find that this can introduce significant uncertainties and thus we restrict the RANS results here to the very high values of Ra^*, where we can verify the correct wall-model implementation. With these caveats, however, we do see reasonable agreement between LES and RANS for $\varphi = 0.9$ at $Ra^* = 10^8$, and, taken together, the LES and RANS results for $\varphi = 0.9$ collapse very well to a power-law behavior. Finally, consider the RANS results for thin gaps with varying values of φ in Figure 8. Here we observe a significant scatter with apparently higher slopes for the highest values of φ. In addition to under predicting the effective conductivity, it appears that Scanlan's modified Rayleigh number does not scale-out the gap diameter ratio for the turbulent case with thin gaps.

To summarize, the simulation results obtained with RANS, LES, and DNS confirm higher gap effective conductivities (lower insulating effect) than

predicted by the Scanlan correlation when the flow is fully turbulent. Looking at the original data Scanlan used to develop the correlation, we see no experimental data for thin gaps with high values of Ra^*; what data does exist at high Ra^* were for thicker gaps and, as we have seen here, such gaps are laminar to much higher Ra^*. Two avenues we are therefore pursuing for future research are (i) to develop a more reliable empirical formula to reliably estimate the gap effective conductivity under conditions relevant to the Titan Montgolfiere, and (ii) extend the RANS modeling now to full-scale balloons, while maintaining careful control over potential grid and modeling errors associated with the thin turbulent boundary layers in the gap.

2.4. Buoyancy performance with forced external convection for Titan flights

It is important to quantify the heat losses due to forced convection when the balloon is in motion. Vertical motion with respect to the atmosphere is most likely and will occur both during the initial inflation and heat-up of the balloon upon arrival and during commanded altitude changes during the science mission itself. These vertical velocities will be small (few meters/sec) due to the weak gravity and large inertia of the balloon. Nevertheless, some additional heat loss will occur due to the forced convection outside the balloon and it is necessary to quantify this.

In this section we consider a full scale 10 m diameter double-wall balloon with a 0.2 m gap and a RPS to heat the inner volume. The system total dry mass is specified to be 200 kg.

The standard engineering model for the external free (natural) convection on sphere is the Campo model. [12] In this model, the Nusselt number is a direct function of the Rayleigh number:

Campo (Ra>1.5 x 10^8):

$$\mathrm{Nu}_{\mathrm{ext}} = 0.10 Ra^{0.340} \qquad (1)$$

From the CFD results, one may integrate in space the wall quantities to obtain the integrated wall temperature and heat flux. This integration yields overall 1D values; from the wall heat flux q_{ext} and external wall temperature $T_{w,ext}$, one looks for an expression of the form:

$$\mathrm{Nu}_{\mathrm{ext}} = \theta_{\mathrm{ext}} \mathrm{Ra}^{0.340} \qquad \mathbf{(2)}$$

where θ_{ext} is a coefficient to be found.

A set of CFD computations was done using varying heating power: Q_{RTG} = 325, 434, 868, 1305, 1740 [W] for the shaped Titan balloon with a ceiling flight at 8 km. An example for the flow field obtained with a 1 m/s external flow field at 8 km altitude is presented in Fig. 9.

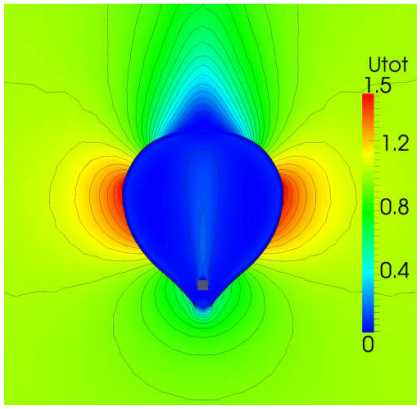

Fig. 9: Velocity flow field for the 1 m/s forced descent with low RTG heating (1305 W).

Parameter matching the CFD results to an equation of the form in Eq. (2) gives:

$$\mathrm{Nu}_{\mathrm{ext}} = 0.08 \mathrm{Ra}^{0.340} \qquad \mathbf{(3)}$$

It can be seen that the model for the Nusselt number as a function of Rayleigh obtained from the CFD is very close to the Campo model for spheres from the literature (within 20%). The difference may be attributed to the difference in shapes. This confirms that the CFD computations are realistic and consistent at least for the external flow part.

To compute the forced convection for a Titan Montgolfiere balloon, a set of computations with external velocities at a constant altitude of h=8 km were performed. The velocities ranged from 0 to 1.0 m/s with steps of 0.25 m/s, which is a representative velocity range for the expected balloon vertical motion.

The total Nusselt number usual formulation is a mixture between the free and the forced convection. Once can write:

$$\mathrm{Nu}_{\mathrm{tot}}^{\mathrm{n}} = \mathrm{Nu}_{\mathrm{free}}^{\mathrm{n}} + \mathrm{Nu}_{\mathrm{forced}}^{\mathrm{n}} \qquad \mathbf{(4)}$$

For the forced convection part, it is common to use an expression based on the Reynolds number. The standard formulation is:

$$\mathrm{Nu}_{\mathrm{forced}} = \theta_{\mathrm{forced}} . \mathrm{Re}^{\mathrm{m}} \qquad \mathbf{(5)}$$

There are two coefficients that must be found: on the one hand the power m, on the other hand the scaling θ_{forced}. This is done using computational results.

The heat transfer rate (Nusselt number) depends on the Reynolds number. For the laminar range, the widely accepted McAdams [13] relationship is used. For the higher Reynolds number turbulent regime, an empirical scaling factor is employed according to Carlson and Horn **Error! Reference source not found.**]. The standard forced convection model used for the Titan balloons is then:

$$\mathrm{Nu}_{\mathrm{forced,lami.}} = 0.37\,\mathrm{Re}^{0.60}, \mathrm{Re} < 2.10^5$$
$$\mathrm{Nu}_{\mathrm{forced,turb.}} = 0.74\,\mathrm{Re}^{0.60}, \mathrm{Re} > 2.10^5 \qquad \textbf{(6)}$$

From the computations with external velocities, one may obtain the total Nusselt number. The total number is derived from the wall heat flux on the external wall (w,ext) and the temperature gradient between the ambient (a) and the external wall. These values are computed using integration from the CFD results. Using the external balloon diameter (d_{ext}) and the ambient fluid conductivity (λ_{ext}), the total Nusselt number writes:

$$\mathrm{Nu}_{\mathrm{tot}} = \frac{q_{w,ext}}{\nabla T^{a}_{w,ext}} . \frac{d_{ext}}{\lambda_a} \qquad \textbf{(7)}$$

Inserting Eq. (5) with Eq. (7) into Eq. (3), one may compute the forced convection part from the CFD integrated results. In the end, the forced convection writes:

$$\theta_{\mathrm{forced}} . \mathrm{Re}^{m} = \left[\left[\frac{q_{w,ext}}{\nabla T^{a}_{w,ext}} . \frac{d_{ext}}{\lambda_a}\right]^{n} + [0.08.\mathrm{Ra}^{0.340}]^{n}\right]^{1/n} \qquad \textbf{(8)}$$

Using a mixing coefficient n=3 (corresponding to spheres e.g., [14]), the θ_{forced} coefficient is computed based on several assumptions of the exponent m. Since we are looking for a forced convection law that is valid for the entire velocity range, the choice of m will be based on a constant θ_{forced} value.

From the integrated CFD results, the coefficients are computed and presented in Table 2.

Table 2: forced convection model coefficients.

U [m/s]	m =0.60 θ_{forced}	m =0.70 θ_{forced}	m =0.75 θ_{forced}
0.25	0.85	0.08	0.10
0.50	0.95	0.13	0.10
1.00	1.12	0.23	0.11

It is seen that with an m power of 0.75, the θ_{forced} values do not change much. Therefore, one can propose a forced convection law valid for Titan balloon in the U < 1 m/s range with the following coefficients:

$$\mathrm{Nu}_{\mathrm{forced,lami.}} = 0.37.\mathrm{Re}^{0.60}, \mathrm{Re} < 2.10^5$$
$$\mathrm{Nu}_{\mathrm{forced,turb.}} = 0.10.\mathrm{Re}^{0.75}, \mathrm{Re} > 2.10^5 \qquad \textbf{(9)}$$

This model may seem to differ largely from the forced convection model in Eq. (6); however a comparison for a complete descent and ceiling flight shows that both trajectories are close one another. The main difference lies in the undershoot caused by a higher descent velocities due to the larger convective losses with the present forced convection model. The descent and ceiling flight is presented in Fig. 10. The flight corresponds to a 10 m diameter double wall balloon with a 0.20 m gap spacing, a Q_{RTG}=1740 [W] heat source and a total dry mass of 200 [kg].

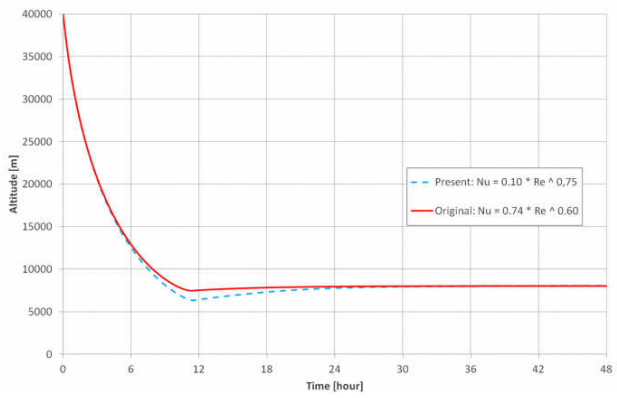

Fig. 10: Comparison of forced convection models on the complete trajectory showing strong similarities in descent velocities. The legend indicates the Nusselt law in the turbulent regime.

It can be noted that the change in slope for the Nusselt number from the laminar (m=0.37) to the turbulent (m=0.75) regimes agrees with the general laws of convection. One may cite the work on heated cylinders [15,16,17] in which the Nusselt formulations follow a very similar trend to the proposed formulation for a Titan balloon in Eq. (9).

Finally, compared to Earth, one should note that because of the atmospheric profile, the external forced heat transfer on the 10 m Titan balloon will almost always be turbulent, even for small external velocities, see Fig. 1.

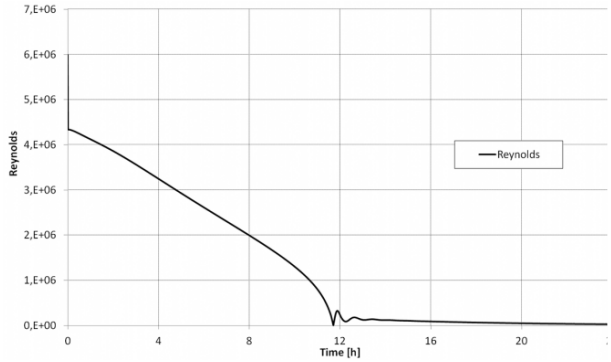

Fig. 11: Reynolds number during Titan descent from injection (40km, -5m/s) to ceiling (8km) for a 10m balloon.

3. PARAMETRIC ASSESSMENT OF FULL SCALE BALLOON DESIGN

The CFD results presented in the previous section lay the foundation for estimating the performance of full scale, double-wall Montgolfiere balloons at Titan. The cryogenic test results provide a good validation for the RANS modeling approach (Section 2.1), the sphere-on-cone geometry calculations show that the perfect sphere approximation adds only a ~3% error (Section 2.2) and the RANS, DNS and LES simulations of spherical gaps support the conclusion that the engineering 1D correlations (Scanlan, Ref. 6) do not adequately cover the turbulent flow regime (Section 2.3 and Fig. 3). The accumulated knowledge from these results and the prior CFD studies [7, 8] have been synthesized into a simplified lumped-mass model for the balloon thermodynamic behavior based on a spherical geometry. This new model is functionally equivalent to that used to design the balloon for TSSM [**Error! Bookmark not defined.**], but with updated parameters to reflect the recent CFD results. The specific heat transfer equations used are those presented in Feldman *et al* [8], Equations 7 through 13, with two modifications:

- The radiative heat transfer is set to zero (Feldman *et al*, [8] Eq. 9) since it contributes little heat flux at 90 K.
- An additional scaling factor of 2.8 is added to the right hand side of Feldman *et al* [8] Equation 8 to account for the reduced thermal insulation performance of the gap as per the results of Fig. 3 above.

The resulting equations were coded up and solved numerically in a trade study that looked at the design tradeoff between balloon size and payload mass as a function of equilibrium float altitude for different heating levels. The trade study specified the following parameters:

- Double-wall balloon with a 0.1 m gap between the inner and outer walls.
- 0.05 kg/m^2 average areal density of the balloon material, including seams and structural reinforcements.
- 100% nitrogen atmosphere composition with real gas properties as a function of temperature and pressure.
- Three different heating levels of 630, 1088 and 1740 W. The highest value corresponds to the heat output of an MMRTG after 15 years, and the lowest heat output corresponds to 2 ASRGs after 15 years.
- Three different balloon diameters of 12, 13 and 14 m.

The results are shown in Fig. 12 along with a data point for the TSSM design. The TSSM balloon was 10.6 m in diameter, but the new calculation shows that a 12 m balloon is now required to provide the ~220 kg of non-balloon lift mass with the same heating value of 1740 W. This 45% increase in the balloon volume directly results from the effect of decreased gap insulation for the new calculation as compared to the original TSSM model.

It can be seen that there is a relatively weak effect in the increase in non-balloon lift mass as a function of increasing balloon diameter: each 1 m diameter increase adds approximately 25 kg of payload at 1740 W but only 10 kg of payload at 630 W. There is no hard upper limit to the allowable size of a Titan Montgolfiere balloon, but anything larger than 15 or 16 m will encounter difficulties with mass and storage volume inside the aeroshell. Even at that size, it is clear that the 630 W heating level will not provide 200+ kg of non-balloon lift mass typical of TSSM-like flagship missions. Such payloads are achievable with the 1088 W case at ~15 m diameter, while the 1740 W of the MMRTG can clearly support these payload masses and more.

It should be noted that ongoing work with LES simulations for the gap heat transfer may result in modifications to these results that are based on the generally less accurate RANS simulations used to construct Fig. 3. Until such time, however, Fig. 12 provides a good estimate for the design space of Titan Montgolfiere balloons.

4. CONCLUSIONS

Results have been presented for validated CFD simulations of Titan Montgolfiere (hot air) balloons. It was discovered that the gap in a double-wall balloon design provides less thermal insulation than were previously expected based on engineering correlations derived from small scale laboratory experiments with

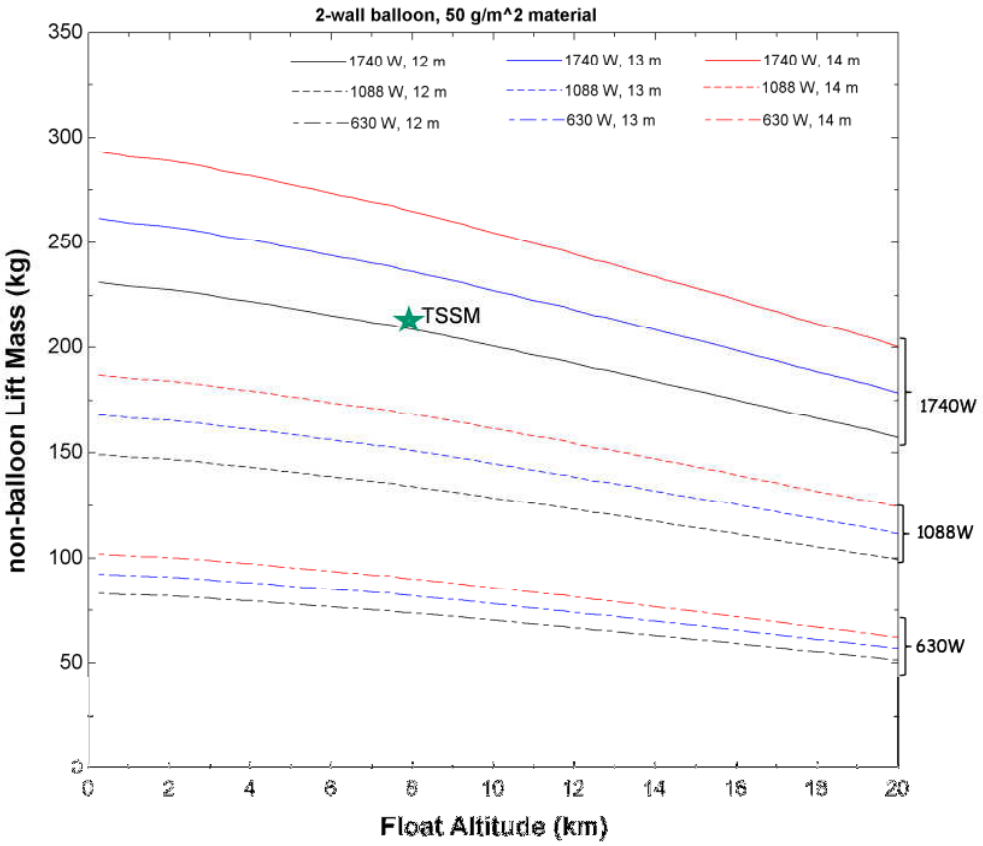

Fig. 12: Full-scale Titan Montgolfiere design curves for a double-wall balloon at 8 km float altitude and with three different heating values from the RPS (640, 1088 and 1740 W). The TSSM design point is shown for reference.

heated metal spheres. Calculations with a more realistic sphere-on-cone geometry and open hole at the bottom of the balloon showed only a small 3% reduction in estimated buoyancy as compared to perfect spheres. The addition of forced convection effects had only a small effect on balloon performance: the limiting case of a newly deployed balloon heating up for the first time in the atmosphere was able to arrest its descent with a 2 km trajectory undershoot before settling out at the equilibrium float altitude of 8 km. Finally, design curves were presented for the full scale Titan Montgolfiere balloon that incorporate the latest CFD results. The decreased insulation performance of the gap translates into the need for larger balloons than previously expected: the example of the TSSM mission showed a balloon diameter increase from 10.6 to 12 m diameter for the same heating level and payload mass.

5. ACKNOWLEDGEMENTS

The US-based research described in this paper was carried out at the California Institute of Technology and at the Jet Propulsion Laboratory, California Institute of Technology, under a contract with the National Aeronautics and Space Administration.

6. REFERENCES

[1] Ralph D. Lorenz, "A Review Of Balloon Concepts For Titan", JBIS, Vol. 61, pp 2-13, 2008.

[2] G. E. Dorrington, "Concept options for the aerial survey of Titan", *Advances in Space Research*, Vol. 47, pp. 1-19, 2011.

[3] Jeffery L. Hall, "A Survey of Titan Balloon Concepts and Technology Status", AIAA Paper 2011-6867.

[4] National Academy Space Studies Board, "Visions and Voyages for Planetary Science in the Decade 2013-2023", United States National Research Council, March 7, 2011.

[5] Kim Reh, Christian Erd, Dennis Matson, Athena Coustenis, Jonathan Lunine, Jean-Pierre Lebreton, (2009). "Titan-Saturn System Mission (TSSM) Joint Summary Report", published by NASA and ESA on January 16, 2009. Retrievable at: http://opfm.jpl.nasa.gov/files/TSSM_Joint%20Summary%20Report_Public%20Version_090120.pdf.

[6] Scanlan, J., Bishop, E., and Powe, R., "Natural convection heat transfer between concentric spheres", *Int. J. Heat Mass Transfer* , Vol. 13, No. 12, 1970, pp. 1857–1872.

[7] Arnab Samanta, Daniel Appelo, Tim Colonius, Julian Nott and Jeffery Hall (2010), "Computational Modeling and Experiments of Natural Convection for a Titan Montgolfiere," AIAA Journal, Vol. 48, No. 5, May 2010.

[8] Yuri Feldman, Tim Colonius, Michael Pauken, Jeffery L. Hall, Jack A. Jones, "Numerical and Experimental Modeling of Natural Convection for a Cryogenic Prototype of a Titan Mongolfiere", AIAA Paper 2011-6869, AIAA Balloon Systems Conference, Virginia Beach, VA, September 20-22, 2011.

[9] Ansys Fluent 12 Theory Guide, Ansys Inc (US), https://www.sharcnet.ca/Software/Fluent12/html/th/node3.htm, 2009.

[10] http://www.openfoam.com/.

[11] Germano, M., Piomelli, U., Moin, P., and Cabot, W., "A dynamic sub-grid scale eddy viscosity model", *Physics of Fluids A*, Vol. 3, 1991, pp. 1760–1765.

[12] Campo, Correlation equation for laminar and turbulent natural-convection from spheres, *Warme Und Stoffubertragung-Thermo and Fluid Dynamics*, Vol. 13, No. 1-2, 1980, pp. 93–96.

[13] McAdams, W. H., "Heat Transmission", *McGraw-Hill, New York*, 1954.

[14] Incropera, DeWitt, Bergman, Lavine, "Fundamentals of Heat and Mass Transfer, 6th edition", (c) 2007 John Wiley & Sons, Inc.

[15] Hilpert, R. "Heat Transfer from Cylinders," Forsch. Geb. Ingenieurwes, 1933.

[16] Fand, R. M. and K. K. Keswani. "A Continuous Correlation Equation for Heat Transfer from Cylinders to Air in Crossflow for Reynold's Numbers from 10-2 to 2(10)5," *International Journal of Heat and Mass Transfer*, 1972.

[17] Zukauskas, A. "Heat Transfer From Tubes in Crossflow," *Advances in Heat Transfer*, 1987.